Bioorganic Chemistry 93 (2019) 103289

Contents lists available at ScienceDirect

Bioorganic Chemistry

journal homepage: www.elsevier.com/locate/bioorg

Microwave synthesis of novel halogenated β-enaminonitriles linked 9-bromo-1*H*-benzo[*f*]chromene moieties: Induces cell cycle arrest and apoptosis in human cancer cells via dual inhibition of topoisomerase I and II

Ahmed M. Fouda[a], Mohammed A. Assiri[a], Ahmed Mora[b], Tarik E. Ali[a,c], Tarek H. Afifi[d], Ahmed M. El-Agrody[b,*]

[a] Chemistry Department, Faculty of Science, King Khalid University, Abha 61413, Saudi Arabia
[b] Chemistry Department, Faculty of Science, Al-Azhar University, Cairo 11884, Egypt
[c] Department of Chemistry, Faculty of Education, Ain Shams University, Roxy, Cairo, Egypt
[d] Chemistry Department, Faculty of Science, Taibah University, Al-Madinah Al-Munawarah 30002, Saudi Arabia

ARTICLE INFO

Keywords:
Microwave synthesis
Benzochromenes
Antitumor activity
Cell cycle analysis
Topoisomerase
SAR study

ABSTRACT

A novel series of halogenated β-enaminonitriles (**4a-m**), linked 9-bromo-1*H*-benzo[*f*]-hromene moieties, were synthesized via microwave irradiation and were predestined for their cytotoxic activity versus three cancer cell lines, namely: MCF-7, HCT-116, and HepG-2. Several of the tested compounds showed high growth inhibitory activities versus the tumor cell lines. Particularly, compounds **4c**, **4d**, **4f**, **4h**, **4j**, **4l**, and **4m** demonstrated superior antitumor activities against the aforementioned cell lines. Moreover, the apoptosis process in all the tested cells was induced by compounds **4c**, **4d**, **4h**, **4l**, and **4m**, as observed by the Annexin V/PI double staining flow cytometric assay. The DNA flow, cytometric analysis revealed that these compounds prompted cell cycle arrest at the G2/M phases. Furthermore, the topoisomerase catalytic activity assays indicated that these compounds inhibited both the topoisomerase I and II enzymes.

1. Introduction

Microwave heating through dielectric losses has been utilized in synthetic organic chemistry, as it allows the transformations to proceed faster, safer, and with a lower energy input, which in turn speeds organic reactions, develops product pureness, and facilitates the work-up [1–7]. Multicomponent reactions are assisting steps for initiating new organic materials in good yields [8–13]. A variety of natural and synthesized 4*H*-chromenes and 4*H*-benzochromenes are used as effective reagents against asthma, anti-trypanosomal, arthritis, depression, anxiety, loss of appetite, Alzheimer's, Schizophrenia disorder, and other disorders of the central nervous system, diabetic complications and changes in blood pressure [14–19]. However, the substituted 4*H*-benzo[*h*]chromenes are biologically remarkable compounds that possess an assortment of pharmacological activities. For instance, 2-amino-4-(4-chloro/2- or 4-nitrophenyl)-4*H*-benzo[*h*]chromene-2-carbonitriles (**A**), have effective cytotoxic and apoptotic behaviors against different cell lines: MCF-7,MDA-MB-231, HepG-2, T-47D, SK-*N*-MC, KB, and PC3 [20]; 2-amino-4-aryl-6-chloro/methoxy-4*H*-benzo[*h*]chromene-3-carbonitriles (**B**), has been reported as active cytotoxic agents against breast adenocarcinoma (MCF-7), human colon carcinoma (HCT-116) and hepatocellular carcinoma (HepG-2) [21,22]. 2-Amino-5,6-dihydro-8-methoxy-4-phenyl-4*H*-benzo[*h*]chromene-3-carbonitriles (**C**) reported as active cytotoxic agents against human glioblastoma cells [23] while, 2-amino-4-aryl-4*H*-benzo[*h*]chromene-2-carbonitriles (**D**) exhibits antiproliferative activities and *c-Src* kinase inhibitor [24,25]. Moreover, 4-phenyl-2-(*N*-succinimido)-4*H*-benzo[*h*]chromene-3-carbonitriles (**E**) displays anti-rheumatic activity and 4-aryl-2,7-diamino-4*H*-benzo[*h*]chromene-3-carbonitriles (**F**) has been reported as an active antitumor agent [26,27], Fig. 1.

Furthermore, a range of studies has revealed the potential of 1*H*-benzo[*f*]chromene derivatives. As an example, 3-amino-8-bromo-1-(4-chlorophenyl)-1*H*-benzo[*f*]chromene-2-carbonitrile and 3-amino-1-aryl-1*H*-benzo[*f*]chromene-2-carbonitriles (**G**) exhibits *c-Src* kinase inhibitory and antiproliferative activities [13,24]; 1*H*-benzo[*f*]chromene derivatives (**H**) demonstrates a high potency for the hAChE inhibitors [28]. The 1*H*-benzo[*f*]chromene derivatives (**I**) operates as a blood-brain barrier with low toxicity [28] whereas, the 1-aryl-2-(1*H*-tetrazol-5-yl)-1*H*-benzo[*f*]chromene-3-amines (**J**) perform as an anticancer agent [29]. The 3,5-diamino-1-phenyl-1*H*-benzo[*f*]chromene-2-

* Corresponding author.
E-mail address: elagrody_am@yahoo.com (A.M. El-Agrody).

https://doi.org/10.1016/j.bioorg.2019.103289
Received 15 July 2019; Received in revised form 22 August 2019; Accepted 16 September 2019
Available online 20 September 2019

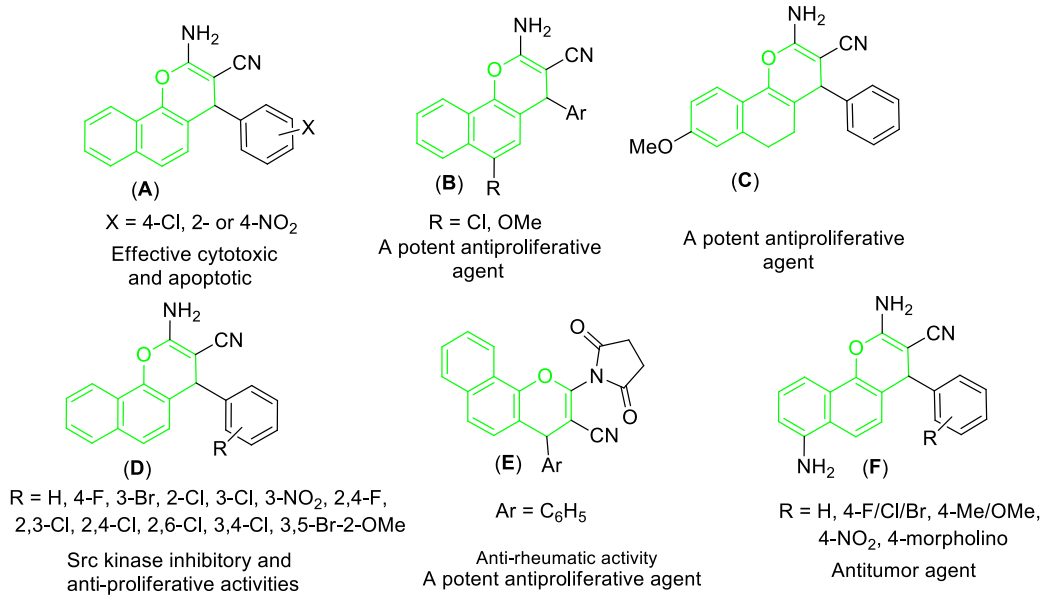

Fig. 1. Structure of some 4*H*-benzo[*h*]chromene derivatives (Green highlighted) with cytotoxic and apoptotic effects. (For interpretation of the references to colour in this figure legend, the reader is referred to the web version of this article.)

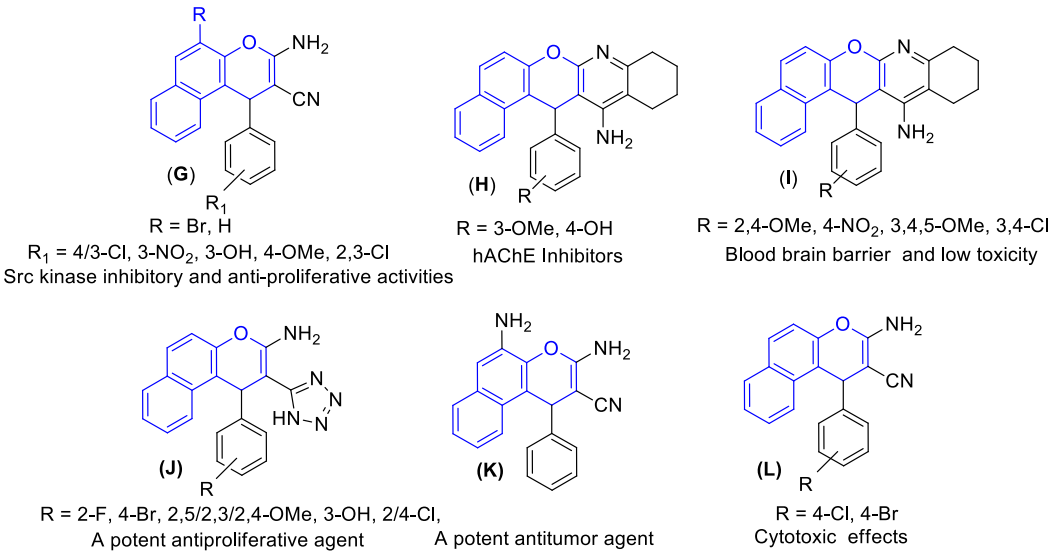

Fig. 2. Structure of some 1*H*-benzo[*f*]chromene derivatives (blue highlighted) with cytotoxic and apoptotic effects. (For interpretation of the references to colour in this figure legend, the reader is referred to the web version of this article.)

carbonitriles (**K**) acts as an antitumor agent [26], and 3-amino-1-(4-chloro/bromophenyl)-1*H*-benzo[*f*]chromene-2-carbonitriles (**L**) has been reported as an active cytotoxic and apoptotic effect against a variety of cell types [20], as presented in Fig. 2.

Additionally, a number of chemotherapeutic factors that generate chemotherapeutic action through their aptitude to inhibit nuclear DNA topoisomerases (Topos) have been the mainstay of cancer treatment [30]. Topos is evolutionarily protected nuclear enzymes, which are vital for DNA metabolism, and are embroiled in creating the indispensable topological state of DNA during replication, transcription, recombination, and chromatin remodeling [31,32].

Considering the great potential of the biological activities of the 2-aminobenzochromenes [20–29], we, herein, are reporting the synthesis, cytotoxic activity, and structural activity relationship (SAR) of the novel series of halogenated *β*-enaminonitriles. Further studies were incorporated for the most potent synthesized derivatives, discussing their mechanism of action, ability to cause cell cycle arrest, and ability to induce apoptosis in tumor cells against MCF-7, HCT-116, and HepG-2 cell lines. The inhibitory influence of these effective compounds on the catalytic activity of the topoisomerase enzymes I and II will be investigated.

2. Results and discussion

2.1. Chemistry

This work exploits the highly efficient one-pot, three-component synthetic methodology to generate a variety of halogenated 3-amino-9-bromo-1-aryl-1*H*-benzo[*f*]chromene-2-carbonitrile (**4a-m**) by the reaction of 7-bromo-2-naphthol (**1**) with a diversity of aromatic aldehydes (**2a-m**) and malononitrile (**3**) in an ethanolic/piperidine solution under microwave irradiation conditions for 2 min at 140 °C, as presented in Scheme 1. The maximum power of the microwave irradiation was optimized by repeating the reaction at different watt powers and time.

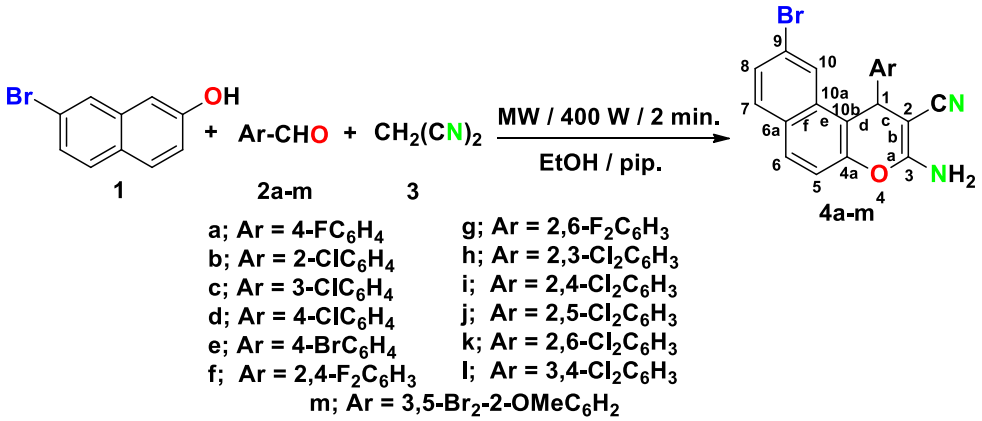

Scheme 1. Synthesis of halogenated 1*H*-benzo[*f*]chromene derivatives (**4a-m**).

The microwave radiations at 400 W and a reaction time of 2 min gave the highest yield.

Both the spectroscopic data and the elemental analyses were consistent with the structures. The IR spectra of compounds **4a-m** disclosed absorption bands around υ 3479–3439, 3337–3319, 3290–3204 cm^{-1} for NH_2 in addition to the absorption bands of the cyano groups in the region υ 2202–1995 cm^{-1}. On the other hand, the ^1H NMR spectra of **4a-m** divulged the signals of the methine proton in the range of δ 6.10–5.34 ppm and the methoxy group at δ 3.77 for compound **4 m**. Moreover, the ^1H NMR spectra revealed the presence of the D_2O exchangeable NH_2 protons in the range of δ 7.20–7.00 ppm. The ^{13}C NMR spectra of **4a-m** showed signals resonating in the range of δ 39.03–27.94 ppm, attributed to the CH carbons, and at δ 61.89 ppm, ascribed to the CH_3 carbon for compound **4m**. In addition, the MS spectra of **4a-m**, the ^{13}C NMR-DEPT spectra at 45°, 90°, 135°, and the ^{13}C NMR-APT spectra of compound **4g**, **4j**, **4l**, and **4 m** delivered the absolute confirmation for their structures (see supplementary materials).

2.2. Biological activity

2.2.1. In vitro cytotoxic activity

In this research, newly synthesized compounds, 3-amino-9-bromo-1-aryl-1*H*-benzo[*f*]chromene-2-carbonitriles (**4a-m**) were subjected to cytotoxic evaluation against the selected human cancer cell lines, specifically: mammary gland breast cancer (MCF-7), human colon cancer (HCT-116), and human hepatocellular carcinoma (HepG-2) with Vinblastine and Doxorubicin as a reference drug using the MTT assay [33–35]. The *in-vitro* cytotoxicity evaluation was achieved under different concentrations (50 μg/mL, 25 μg/mL, 12.5 μg/mL, 6.25 μg/mL, 3.125 μg/mL, 1.56 μg/mL and 0 μg/mL) at Al-Azhar University. The results were expressed as growth inhibitory concentration (IC_{50}) values that represent the necessitated concentrations of the compounds to produce a 50% inhibition of cell growth after 24 h of incubation, in comparison to the untreated controls and are summarized in Fig. 3 and Table 1.

Table 1 explains that most of the targeted compounds are labeled with excellent, strong, or modest growth inhibitory activities against the assessed cancer cell lines. Examinations of the cytotoxicity versus different cell lines denoted that HepG-2 was the most sensitive cell line to the influence of the novel derivatives. Compounds **4h** and **4f** (IC_{50} = 0.49 ± 0.21 and 1.52 ± 0.11 μg/m proved to be the most potent derivatives above all the tested compounds against the MCF-7 cell line when evaluated against Vinblastine and Doxorubicin (IC_{50} = 3.28 ± 0.03 and 0.39 ± 0.01 μg/mL) while compounds **4m**, **4h**, **4d**, and **4c** (IC_{50} = 0.58 ± 0.15, 0.64 ± 0.1, 0.8 ± 0.12 and 1.36 ± 0.4 μg/mL, respectively) were more potent and efficacious than Vinblastine and Doxorubicin (IC_{50} = 14.03 ± 0.08 and 2.15 ± 0.15 μg/mL) against the HCT-116 tumor line. Additionally, the cytotoxicity evaluation of the HepG-2 cell line revealed that compound **4l** (IC_{50} = 0.47 ± 0.01 μg/mL) was the most potent derivative from all the tested compounds and the standard drug Doxorubicin (IC_{50} = 0.62 ± 0.04 μg/mL) whereas compounds **4l**, **4m**, **4c**, **4g**, **4j**, **4a**, **4d**, and **4f** (IC_{50} = 0.47 ± 0.01, 0.71 ± 0.6, 0.77 ± 0.14, 0.9 ± 0.2, 1.07 ± 0.3, 1.26 ± 0.03, 1.67 ± 0.23 and 2.51 ± 0.7 μg/mL, respectively) were more active than Vinblastine (IC_{50} = 2.58 ± 0.01 μg/mL).

2.2.2. G2/M phase cell cycle arrest in treating cancer cells

Normal cell growth and cell divisions are under the manipulation of four cell cycle stages (G1, S, G2, and M). However, most cancer cells undergo unscheduled cell divisions by the down regulation of the cell cycle. Therefore, the development of anti-cancer therapeutic agents, targeting specific steps of the cell cycle, represents an important therapeutic intervention in treating proliferative diseases like cancer [36,37]. In order to elucidate the effect of the most potent newly synthesized compounds (**4c**, **4d**, **4h**, **4l**, **4m**) against the sundry tumor cell lines, DNA content was analyzed by the flow cytometry, exploiting the FACS Calibers (Becton Dickinson). The distribution of cells along the G1 (2n), G2/M (4n), and S (2n to 4n) phases of the cycle was exhibited in the representative cell cycle distribution histogram of the stained DNA in Fig. 4a. The MCF-7, HCT-116, and HepG-2 cancer cells were remedied with each derivative at its IC_{50} values for 24 h, a controlled experiment with no treatment done. The outcomes on regulating cell cycle progression demonstrated that all the tested compounds have expressed a significant increased percentage (50%) of cells at the G2/M phase in comparison to the 15% in control cells. In addition, these results were accompanied by a considerable decrease in percentage at the G1 and S phases compared to the untreated control cells (Fig. 4b). The cell cycle evaluation presented that the tested derivatives significantly arrested the cells' progression by restricting the G2/M phases.

2.2.3. Apoptosis induction in treating cancer cells

Many anticancer compounds exerted their effects by blocking the cell cycle progression, by inducing apoptosis, or the combined effect of both. To further assess the pivotal relationship of the cell cycle arrest and apoptosis to the newly synthesized tumor suppression compounds, the Phosphatidylserine (PS) translocation to the cell membrane as a marker for apoptosis was measured by the means of the Annexin V/PI double staining flow cytometric assay [38]. The representative dot plots of the double stained cells (MCF-7, HCT-116, and HepG-2), after treatment with the diverse examined compounds as displayed in Fig. 5a. Unlike necrosis, which was not observed in all the results, all of the treated cells illustrated up to 20% in total apoptosis in evaluation against the 2% of the untreated cells. Moreover, all the tested compounds showed early (Annexin V positive, PI negative) as well as late

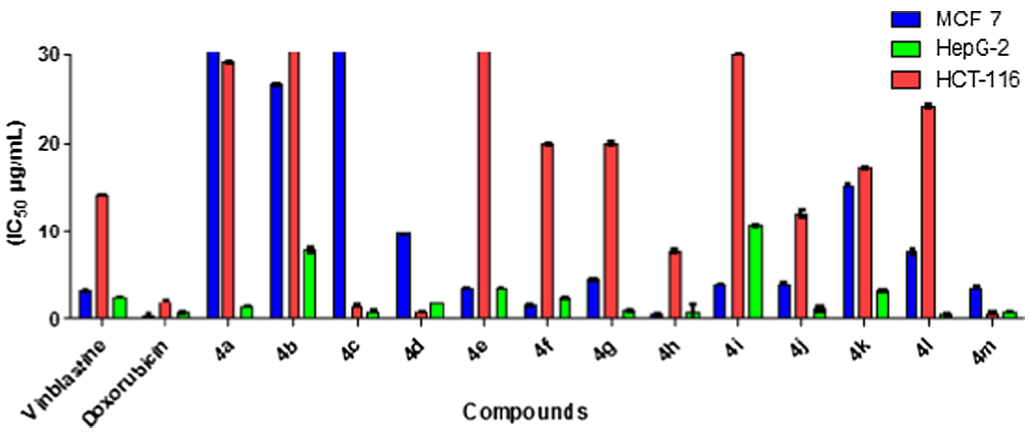

Fig. 3. IC_{50} values are expressed in (µg/ml) of 3-amino-9-bromo-1-aryl-1*H*-benzo[*f*]chromene-2-carbonitrile (**4a-m)** against MCF-7, HCT-116, and HepG-2 tumor cells.

(Annexin V positive, PI positive) apoptosis in, of all the treated cells (Fig. 5b). In other studies, it was established that the Annexin V single positive cells appeared after treatment with early anticancer drugs such as Etoposide and Cytarabine, but not with late anticancer drugs such as Doxorubicin and Methotrexate [39,40]. Our results proposed that the induction of cytotoxicity occurs through mechanisms associated with apoptosis.

2.2.4. Dual inhibitory effects on topoisomerase I and II

Many DNA-binding derivatives exhibit their major pharmacological effect through the interference with the activity of Topoisomerases [41]. As an instance, the delayed onset of mitosis (G2 block) is regularly observed in cells that have been exposed to the Topo blockers [42]. The effects of the synthesized compounds on the topoisomerases I and II enzymes were measured to investigate whether the derivatives that exhibited cytotoxic behavior are Topos catalytic inhibitors. The influence of our compounds on the catalytic activity of Topo I was tested, employing the relaxation assay, while the decatenation assay was exercised for Topo II, which was utilized based on the conversion of the catenated DNA to its decatenated form, as demonstrated in the method. All of the analyzed compounds with the exploitation of the c-MET reference drug has presented the inhibitory DNA relaxation activity of Topo 1 and II in a dose-dependent manner, judged by a decrease in the relaxed DNA and a decrease in the decatenation of KDNA, respectively (Fig. 6a & b). Additionally, compounds **4c** and **4l** have shown the highest inhibitory effect on Topo I and II, respectively. However, the calculated IC_{50} for Topo I was more or less the same for Topo II for each of the tested compounds (Fig. 6c). Taken together, this data indicated that the newly produced derivatives inhibit both the Topo I and Topo II *in vitro* activities. The reactivity of the synthesized compounds, exhibiting dual inhibitors that target both topoisomerase I and II, is attributed to the structural motifs present on both enzymes or their binding to an intercalate DNA.

2.3. SAR studies

The SAR studies the effect of the different substituents (halogen atoms or methoxy group), on the phenyl group (Ar, Scheme 1) at the 1-position of the 1*H*-benzo[*f*]chromene moiety, on the antitumor activities. In comparison to the cytotoxic activities of the three series: the

Table 1
Cytotoxic activity of the target compounds against MCF-7, HCT-116, and HepG-2 cell lines.

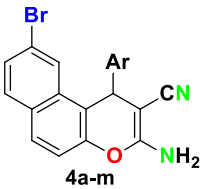

4a-m

Compound	Ar	IC_{50} (µg/mL)[a]		
		MCF-7	HCT-116	HepG-2
4a	4-FC_6H_4	35.98 ± 0.12	29.14 ± 0.11	1.26 ± 0.03
4b	2-ClC_6H_4	26.55 ± 0.5	43.09 ± 0.16	7.79 ± 0.35
4c	3-ClC_6H_4	45.77 ± 0.2	1.36 ± 0.4	0.77 ± 0.14
4d	4-ClC_6H_4	9.63 ± 0.11	0.8 ± 0.12	1.67 ± 0.23
4e	4-BrC_6H_4	3.63 ± 0.14	49.93 ± 0.35	3.6 ± 0.02
4f	2,4-$F_2C_6H_3$	1.52 ± 0.11	19.83 ± 0.2	2.51 ± 0.7
4g	2,6-$F_2C_6H_3$	4.51 ± 0.12	19.92 ± 0.1	0.9 ± 0.2
4h	2,3-$Cl_2C_6H_3$	0.49 ± 0.21	0.64 ± 0.1	7.59 ± 0.17
4i	2,4-$Cl_2C_6H_3$	4.04 ± 0.02	30.09 ± 0.14	10.66 ± 0.15
4j	2,5-$Cl_2C_6H_3$	4.05 ± 0.1	12.88 ± 0.2	1.07 ± 0.3
4k	2,6-$Cl_2C_6H_3$	15.1 ± 0.17	17.15 ± 0.18	3.31 ± 0.16
4l	3,4-$Cl_2C_6H_3$	7.61 ± 0.3	25 ± 0.02	0.47 ± 0.01
4m	3,5-Br_2-2-$OMeC_6H_2$	3.67 ± 0.13	0.58 ± 0.15	0.71 ± 0.6
Vinblastine	–	3.28 ± 0.03	14.03 ± 0.08	2.58 ± 0.01
Doxorubicin	–	0.39 ± 0.01	2.15 ± 0.15	0.62 ± 0.04

[a] IC_{50} values are expressed in µg/mL as the mean values of triplicate wells from at least three experiments and are reported as the mean ± standard error.

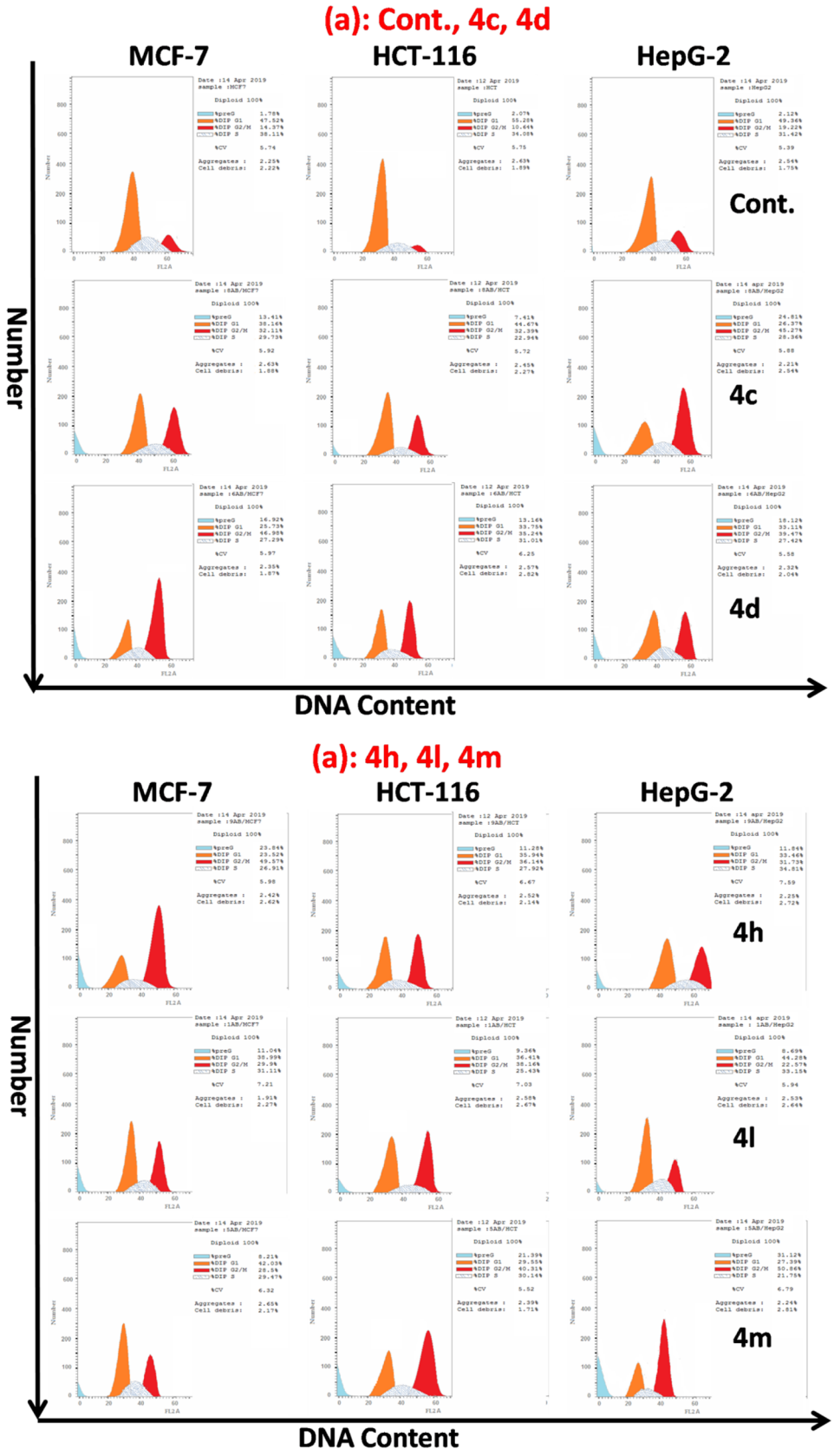

Fig. 4. Effects of compounds **4c**, **4d**, **4h**, **4l**, and **4m** on the cell cycle phases of MCF-7, HCT-116, and HepG-2 cells. **(a)** Representative histograms of the DNA content distribution of cells were incubated with IC_{50} values for 24 h and stained with propidium iodide (PI). Their DNA content was analyzed by the fluorescence flow cytometry. **(b)** The percentage of MCF-7, HCT-116, and HepG-2 cells in the G1, S, and G2/M phases after incubation with compounds **4c**, **4d**, **4h**, **4l**, and **4m** (IC_{50} value) for 24 h. The data are expressed as the mean ± SD of three independent experiments in triplicate.

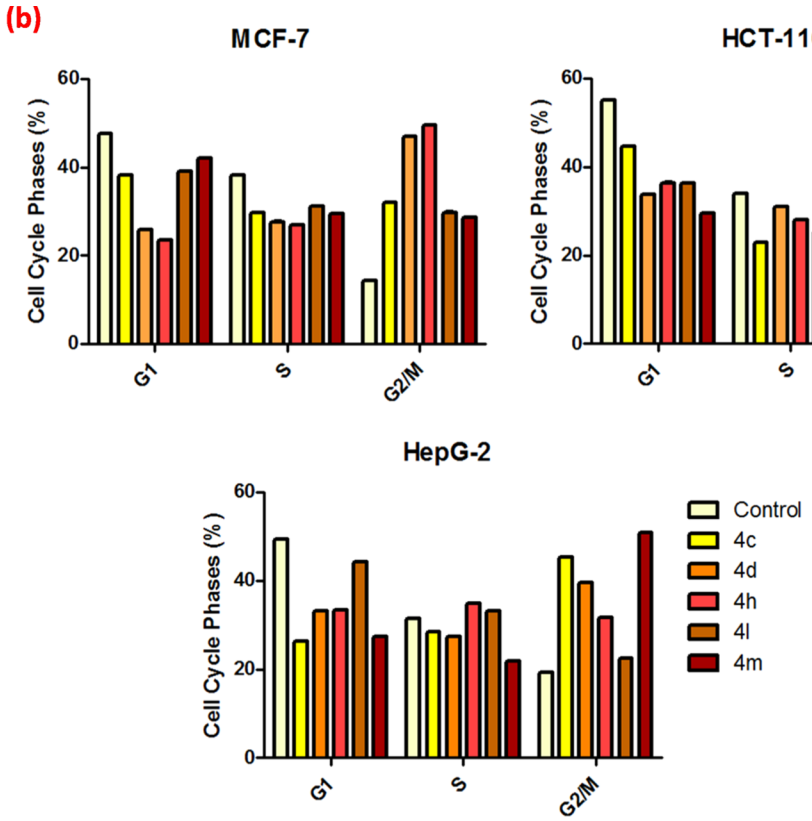

Fig. 4. (*continued*)

mono-, di-, and tri-substituents (**4a-e**, **4f-l**, and **4m**), against MCF-7, it was found that the halogenated disubstituents (second series), like 2,3-Cl_2 and 2,4-F_2, on the phenyl ring of compounds **4h** and **4f** (IC_{50} = 0.49 ± 0.21 and 1.52 ± 0.11 μg/mL) had a much more significant impact on the activities than the first series (**4a-e**) and the third series (**4m**). However, when a comparison is drawn between Vinblastine and Doxorubicin (IC_{50} = 3.28 ± 0.03 and 0.39 ± 0.01 μg/mL) with the MCF-7 cell line, the cytotoxicity was decreased in the order of 2,3-Cl_2 > 2,4-F_2, suggesting that the bulky size of the lipophilic electron-withdrawing disubstituents generates more activity than the other monosubstituents and trisubstituent, respectively. Concerning activity against the HCT-116 cell line, the derivatives **4m**, **4h**, **4d**, and **4c** (IC_{50} = 0.58 ± 0.15, 0.64 ± 0.1, 0.8 ± 0.12 and 1.36 ± 0.4 μg/mL, respectively) were the most active analogs through this study in evaluation against Vinblastine and Doxorubicin (IC_{50} = 14.03 ± 0.08 and 2.15 ± 0.15 μg/mL), hinting that the bulky size of both the lipophilic electron-donating as well as the lipophilic electron-withdrawing substituents (third series, 3,5-Br2-2-OMe) is more beneficial than that of the di- and monosubstituents (2,3-Cl_2, 4-Cl and 3-Cl), respectively. Furthermore, compounds **4l**, **4m**, **4c**, **4g**, **4j**, **4a**, **4d**, and **4f** (IC_{50} = 0.47 ± 0.01, 0.71 ± 0.6, 0.77 ± 0.14, 0.9 ± 0.2, 1.07 ± 0.3, 1.26 ± 0.03, 1.67 ± 0.23 and 2.51 ± 0.7 μg/mL, respectively) displayed excellent activities against the HepG-2 cell line in comparison with Vinblastine and Doxorubicin (IC_{50} = 2.58 ± 0.01 μg/mL and 0.62 ± 0.01 μg/mL), and the activities were decreased in the order of 3,4-Cl_2 > 3,5-Br_2-2-OMe > 3-Cl > 2,6-F_2 > 2,5-Cl_2 > 4-F > 4-Cl > 2,4-F_2, noting that the di-, tri-, and mono-substituents with 3,4-Cl_2, 2,6-F_2, 3,5-Br_2-2-OMe, and 3-Cl have enhanced the activity. Finally, we can deduce that the substitution pattern on the phenyl moiety is a crucial element of the antitumor activity. The incorporation of electron-donating as the methoxy group with electron-withdrawing as the bromine, or with electron-withdrawing chlorine or fluorine at certain position has greatly enriched the activity with the remaining substituents not favorable for this activity.

3. Conclusion

In summary, we have designed and synthesized thirteen novel halogenated *β*-enaminonitrile-based derivatives (**4a-m**), incorporating 9-bromo-1*H*-benzo[*f*]chromene moieties via microwave irradiation conditions, and evaluated their cytotoxicity against three tumor cell lines (MCF-7, HCT-116, and HepG-2). Of these derivatives, compounds **4c, 4d, 4f, 4h, 4j, 4 l,** and **4m** demonstrated superior antitumor activities against the aforementioned cell lines. In particular, compounds **4h** and **4f** displayed the highest activity against MCF-7 cancer cell line with IC_{50} = 0.49 ± 0.21 and 1.52 ± 0.11 μg/m, while compounds **4m, 4h, 4d,** and **4c** displayed excellent growth inhibitory activity against HCT-116 with IC_{50} values ranging from 0.58 to 1.36 μg/mL and compounds **4l, 4m, 4c, 4g, 4j, 4a, 4d,** and **4f** were found the most potent against HepG-2 with IC_{50} = 0.47 to 2.51 ± 0.7 μg/mL as compared with the standard drugs Vinblastine and Doxorubicin. Furthermore, Compounds **4c**, **4d**, **4h**, **4l**, and **4m** afforded the ability to prompt cell cycle arrest at the G2/M phases and incite apoptosis due to the dual inhibitory effect on the catalytic activity of topoisomerase I and II.

4. Experimental section

4.1. Materials and Equipment's

All chemicals were purchased from Sigma-Aldrich Chemical Co. (Sigma-Aldrich Corp., St. Louis, MO, USA). All melting points were measured with a Stuart Scientific Co. Ltd apparatus, which are uncorrected. The IR spectra were recorded on a KBr disc on a Jasco FT/IR 460 plus spectrophotometer. The $^{1}H/^{13}C$ NMR (500/125 MHz) spectra were measured on a BRUKER AV 500 MHz spectrometer in a DMSO-d_6 solvent, using tetramethylsilane (TMS) as an internal standard. The ^{13}C NMR spectra were obtained, using the distortion-free enhancement by the polarization transfer (DEPT) and the attached proton test (APT). Chemical shifts (δ) are expressed in parts per million (ppm). The

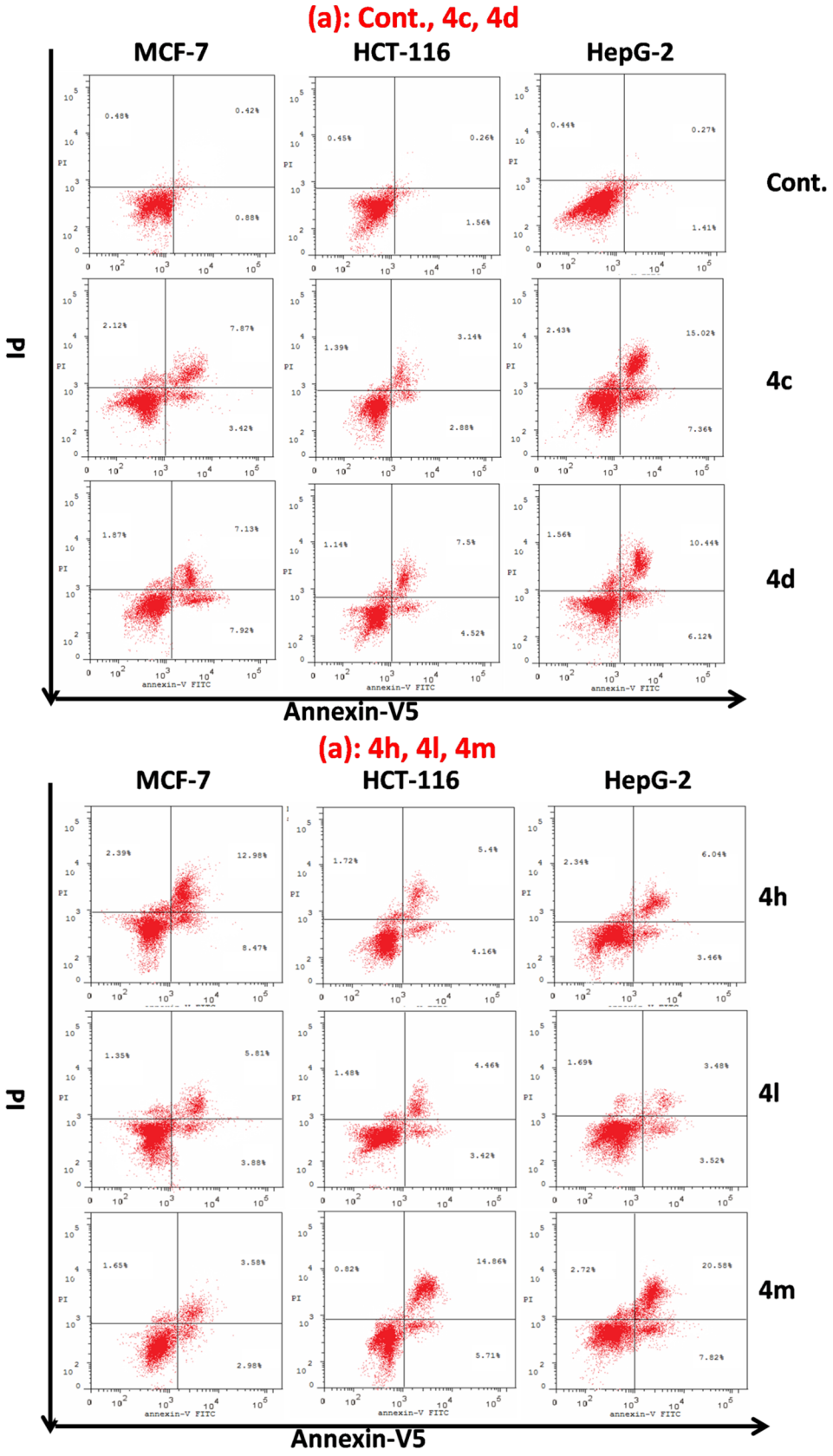

Fig. 5. Apoptosis of MCF-7, HCT-116, and HepG-2 cells treated with compounds **4c**, **4d**, **4h**, **4l**, and **4m**. **(a)** The dot plot of the Annexin V/PI stained cells, treated with the indicated drugs. **(b)** The apoptosis percentage of MCF-7, HCT-116, and HepG-2 cells after incubation with compounds **4c**, **4d**, **4h**, **4l**, and **4m** (IC_{50} value) for 24 h. The data are expressed as the mean ± SD of three independent experiments in triplicate.

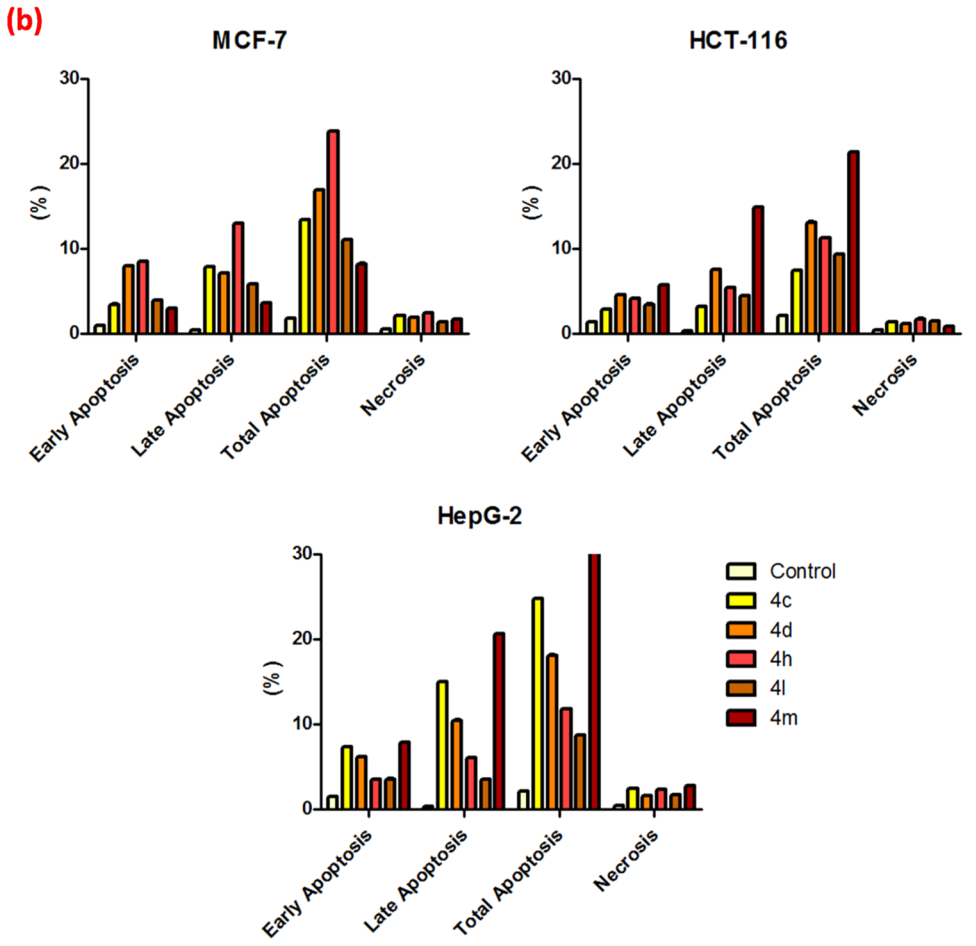

Fig. 5. (*continued*)

Microwave apparatus used is Milestone Sr1, Microsynth. The mass spectra were determined on a Shimadzu GC/MS-QP5050A spectrometer. The elemental analysis was carried out at the Regional Centre for Mycology and Biotechnology (RCMP), Al-Azhar University, Cairo, Egypt; the results were within ± 0.25%. The reaction courses and the product mixtures were routinely monitored by a thin layer chromatography (TLC) on silica gel precoated F_{254} Merck plates.

*4.2. General procedure for synthesis of 1H-benzo[f]chromene derivatives (**4a-m**)*

The reaction mixture of 7-bromo-2-naphthol (**1**) (2.23 g, 0.01 mol), different aromatic aldehydes (**2a-m**) (1.24, 1.4, 1.85, 1.42, 1.75, 2.93 g, 0.01 mol), malononitrile (**3**) (0.01 mol), and piperidine (0.5 ml) in absolute ethanol (30 ml) was heated under microwave irradiation conditions for 2 min at 140 °C. After the completion of the reaction, the mixture of the reaction was cooled to room temperature. The precipitated solid was filtered off, washed with methanol, and recrystallized from ethanol or ethanol/benzene. The physical and spectral data of compounds **4a-m** are as follows:

*4.2.1. 3-Amino-9-bromo-1-(4-fluorophenyl)-1H-benzo[f]chromene-2-carbonitrile (**4a**)*

Yellow crystals from ethanol; yield 91%; m.p. 265–266 °C; IR (KBr) υ (cm^{-1}): 3451, 3332, 3200 (NH_2), 2200 (CN); ^{1}H NMR δ: 8.19–7.42 (m, 9H, aromatic), 7.17 (bs, 2H, NH_2), 5.63 (s, 1H, H-1); ^{13}C NMR δ: 159.78 (C-3), 147.75 (C-4a), 131.37 (C-10a), 130.12 (C-7), 129.43 (C-6a), 128.22 (C-6), 128.15 (C-8), 125.59 (C-10), 124.20 (C-10b), 121.16 (C-9), 119.82 (C-5), 117.54 (CN), 56.65 (C-2), 37.13 (C-1), 152.63, 146.32, 130.75, 113.99 (aromatic); MS *m/z* (%): 396 (M^+ + 2, 18.20), 394 (M^+, 19.17) with a base peak at 215 (100); Anal. Calcd for $C_{20}H_{12}BrFN_2O$: C, 60.78; H, 3.06; N, 7.09. Found: C, 60.71; H, 2.99; N, 7.02%.

*4.2.2. 3-Amino-9-bromo-1-(2-chorophenyl)-1H-benzo[f]chromene-2-carbonitrile (**4b**)*

Yellow crystals from ethanol; yield 94%; m.p. 275–276 °C; IR (KBr) υ (cm^{-1}): 3448, 3330, 3204 (NH_2), 2199 (CN); ^{1}H NMR δ: 7.99–7.04 (m, 9H, aromatic), 7.08 (bs, 2H, NH_2), 5.65 (s, 1H, H-1); ^{13}C NMR δ: 159.58 (C-3), 147.79 (C-4a), 130.81 (C-10a), 130.18 (C-7), 129.56 (C-6a), 128.73 (C-6), 128.00 (C-8), 125.14 (C-10), 121.03 (C-10b), 119.58 (C-9), 117.47 (C-5), 114.19 (CN), 56.72 (C-2), 35.07 (C-1), 142.24, 131.42, 131.00, 129.93, 129.26, 128.27 (aromatic); MS *m/z* (%): 414 (M^+ + 4, 27.07), 412 (M^+ + 2, 100.00), 410 (M^+, 70.97) with a base peak at 412 (100); Anal. Calcd for $C_{20}H_{12}BrClN_2O$: C, 58.35; H, 2.94; N, 6.80. Found: C, 58.28; H, 2.86; N, 6.72%.

*4.2.3. 3-Amino-9-bromo-1-(3-chorophenyl)-1H-benzo[f]chromene-2-carbonitrile (**4c**)*

Yellow crystals from ethanol; yield 91%; m.p. 298–299 °C; IR (KBr) υ (cm^{-1}): 3445, 3331, 3205 (NH_2), 2201 (CN); ^{1}H NMR δ: 8.00–7.05 (m, 9H, aromatic), 7.08 (bs, 2H, NH_2), 5.67 (s, 1H, H-1); ^{13}C NMR δ: 159.58 (C-3), 147.80 (C-4a), 131.00 (C-10a), 130.19 (C-7), 129.94 (C-6a), 128.74 (C-6), 128.28 (C-8), 125.15 (C-10), 121.03 (C-10b), 119.59 (C-9), 117.48 (C-5), 114.20 (CN), 56.24 (C-2), 35.08 (C-1), 142.24, 131.43, 130.83, 129.56, 129.27, 128.01 (aromatic); MS *m/z* (%): 414 (M^+ + 4, 27.74), 412 (M^+ + 2, 100.00), 410 (M^+, 82.66) with a base peak at 412 (100); Anal. Calcd for $C_{20}H_{12}BrClN_2O$: C, 58.35; H, 2.94; N, 6.80. Found: C, 58.43; H, 3.02; N, 6.89%.

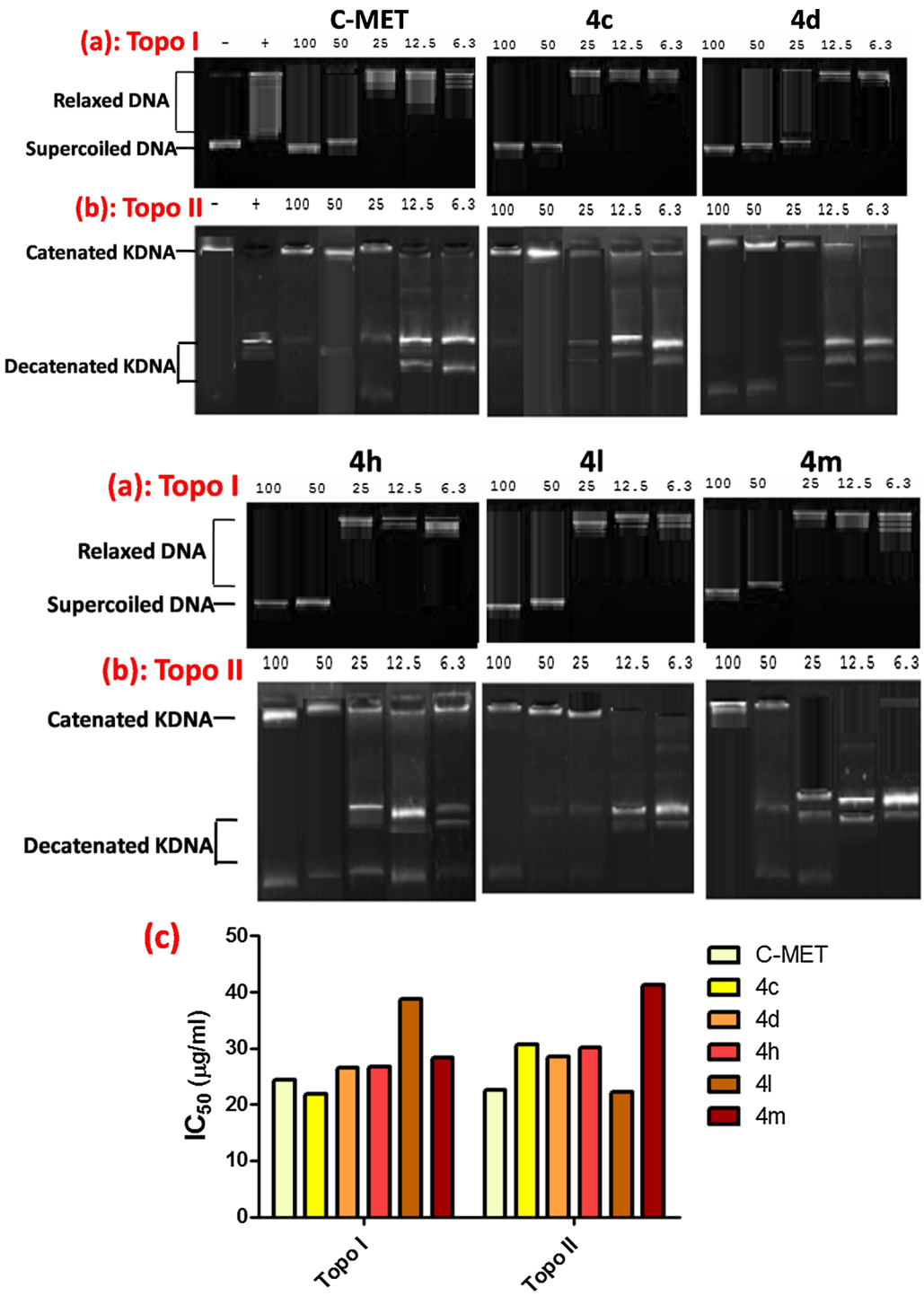

Fig. 6. Dual inhibition of topoisomerase I and II by compounds **4c**, **4d**, **4h**, **4l**, and **4m**. **(a)** Topoisomerase I (Topo I) catalytic activity using supercoiled (Form I) plasmid substrate. **(b)** Topoisomerase II (Topo II) catalytic activity using kineotoplast DNA (kDNA) substrate. Supercoiled plasmid DNA was incubated at 37 °C for 30 min with Topo I enzyme **(a)** or Topo II **(b)** in the presence of various concentrations of indicated compounds. DNA samples were separated by electrophoresis on a 1% agarose gel, stained with ethidium bromide, and visualized by UV light. (−) Substrate DNA alone; (+) Substrate DNA plus 1 unit enzymes. **(c)** IC_{50} values expressed in (μg/ml) for the inhibition of Topoisomerase I and II by compounds (**4c, 4d, 4h, 4l, 4m**).

*4.2.4. 3-Amino-9-bromo-1-(4-chorophenyl)-1H-benzo[f]chromene-2-carbonitrile (**4d**)*

Yellow crystals from ethanol/benzene; yield 93%; m.p. 300–301 °C; IR (KBr) υ (cm^{-1}): 3444, 3333, 3206 (NH_2), 2202 (CN); ^1H NMR δ: 8.02–7.21 (m, 9H, aromatic), 7.05 (bs, 2H, NH_2), 5.42 (s, 1H, H-1); ^{13}C NMR δ: 159.53 (C-3), 147.61 (C-4a), 131.32 (C-10a), 130.69 (C-7), 129.40 (C-6a), 128.77 (C-6), 128.07 (C-8), 125.75 (C-10), 120.96 (C-10b), 120.04 (C-9), 117.48 (C-5), 114.65 (CN), 57.46 (C-2), 39.03 (C-1), 144.40, 131.43, 129.78, 128.78 (aromatic); MS *m/z* (%): 414 ($M^+ + 4$, 13.87), 412 ($M^+ + 2$, 58.63), 410 (M^+, 44.63) with a base peak at 260 (100); Anal. Calcd for $C_{20}H_{12}BrClN_2O$: C, 58.35; H, 2.94; N, 6.80. Found: C, 58.44; H, 3.03; N, 6.90%.

*4.2.5. 3-Amino-9-bromo-1-(4-bromophenyl)-1H-benzo[f]chromene-2-carbonitrile (**4e**)*

Colorless crystals from ethanol; yield 92%; m.p. 250–251 °C; IR (KBr) υ (cm^{-1}): 3441, 3330, 3210 (NH_2), 2203 (CN); ^1H NMR δ: 8.02–7.16 (m, 9H, aromatic), 7.00 (bs, 2H, NH_2), 5.34 (s, 1H, H-1); ^{13}C NMR δ: 159.47 (C-3), 147.61 (C-4a), 130.62 (C-10a), 129.38 (C-7), 128.78 (C-6a), 127.96 (C-6), 126.91 (C-8), 126.74 (C-10), 125.85 (C-10b), 120.21 (C-9), 117.46 (C-5), 115.12 (CN), 57.95 (C-2), 37.68 (C-1), 145.41, 131.54, 129.57, 120.82 (aromatic); MS *m/z* (%): 458 ($M^+ + 4$, 45.04), 456 ($M^+ + 2$, 100.00), 454 (M^+, 49.63) with a base peak at 456 (100); Anal. Calcd for $C_{20}H_{12}Br_2N_2O$: C, 52.66; H, 2.65; N, 6.14. Found: C, 52.53; H, 2.54; N, 6.03%.

*4.2.6. 3-Amino-9-bromo-1-(2,4-difluorophenyl)-1H-benzo[f]chromene-2-carbonitrile (**4f**)*

Colorless crystals from ethanol; yield 86%; m.p. 300–301 °C; IR (KBr) υ (cm^{-1}): 3479, 3337, 3290 (NH_2), 2200 (CN); ^1H NMR δ: 8.64–7.06 (m, 8H, aromatic), 7.15 (bs, 2H, NH_2), 5.79 (s, 1H, H-1); ^{13}C NMR δ: 161.33 (C-3), 159.53 (C-4a), 147.07 (C-10a), 129.71 (C-6a), 130.85 (C-7), 130.72 (C-6), 129.91 (C-8), 129.45 (C-10), 128.56 (C-10b), 123.35 (C-5), 119.83 (C-9), 119.66 (CN), 53.69 (C-2), 28.56 (C-1), 160.13, 159.07, 131.07, 119.58, 117.21, 112.06 (aromatic); MS *m/z* (%): 414 ($M^+ + 2$, 98.75), 412 (M^+, 100.00) with a base peak at 412 (100); Anal. Calcd for $C_{20}H_{11}BrF_2N_2O$: C, 58.13; H, 2.68; N, 6.78. Found: C, 58.20; H, 2.74; N, 6.83%.

*4.2.7. 3-Amino-9-bromo-1-(2,6-difluorophenyl)-1H-benzo[f]chromene-2-carbonitrile (**4g**)*

Pale yellow crystals from ethanol; yield 81%; m.p. 296–297 °C; IR (KBr) υ (cm^{-1}): 3451, 3336, 3222 (NH_2), 2192 (CN); ^1H NMR δ: 8.00–7.07 (m, 8H, aromatic), 7.16 (bs, 2H, NH_2), 5.63 (s, 1H, H-1); ^{13}C NMR δ: 161.15 (C-3), 159.12 (C-4a), 147.92 (C-10a), 131.37 (C-6a), 130.91 (C-7), 129.06 (C-6), 127.86 (C-8), 124.21 (C-10), 121.07 (C-10b), 119.59 (C-9), 119.46 (CN), 117.31 (C-5), 53.63 (C-2), 27.94 (C-1), 160.31, 160.09, 129.98, 119.33, 112.25, 112.09 (aromatic); ^{13}C NMR-DEPT spectrum at 135°CH, CH_3 [positive (up)], CH_2 [negative (down)], revealed the following signals at δ: 130.91 (C-7 ↑), 129.98 (aromatic ↑), 129.06 (C-6 ↑), 127.86 (C-8 ↑), 124.21 (C-10 ↑), 117.31 (C-5 ↑), 112.25 (aromatic ↑), 112.09 (aromatic ↑), 27.94 (C-1 ↑). In the DEPT spectrum at 90° only CH signals are positive (up) and showed δ: 130.91 (C-7 ↑), 129.98 (aromatic ↑), 129.06 (C-6 ↑), 127.86 (C-8 ↑), 124.21 (C-10 ↑), 117.31 (C-5 ↑), 112.25 (aromatic ↑), 112.09 (aromatic ↑), 27.94 (C-1 ↑). In the DEPT spectrum at 45° (CH, CH_2 and CH_3 positive) revealed signals at δ: 130.91 (C-7 ↑), 129.98 (aromatic ↑), 129.06 (C-6 ↑), 127.86 (C-8 ↑), 124.21 (C-10 ↑), 117.31 (C-5 ↑), 112.25 (aromatic ↑), 112.09 (aromatic ↑), 27.94 (C-1 ↑); ^{13}CNMR-APT spectrum CH, CH_3 [positive (up)], CH_2, Cq [negative (down)], revealed the following signals at δ: 161.15 (C-3 ↓), 160.31 (aromatic ↓), 160.09 (aromatic ↓), 159.12 (C-4a ↓), 147.92 (C-10a ↓), 131.37 (C-6a ↓), 130.91 (C-7 ↑), 129.98 (aromatic ↑), 129.06 (C-6 ↑), 127.86 (C-8 ↑), 124.21 (C-10 ↑), 121.07 (C-10b ↓), 119.59 (C-9 ↓), 119.46 (CN ↓), 119.33 (aromatic ↓), 117.31 (C-5 ↑), 112.25 (aromatic ↑), 112.09 (aromatic ↑), 53.63 (C-2 ↓), 27.94 (C-1 ↑); MS *m/z* (%): 414 ($M^+ + 2$, 59.86), 412 (M^+, 62.93) with a base peak at 392 (100); Anal. Calcd for $C_{20}H_{11}BrF_2N_2O$: C, 58.13; H, 2.68; N, 6.78. Found: C, 58.08; H, 2.63; N, 6.72%.

*4.2.8. 3-Amino-9-bromo-1-(2,3-dichlorophenyl)-1H-benzo[f]chromene-2-carbonitrile (**4h**)*

Colorless crystals from ethanol; yield 89%; m.p. 295–296 °C; IR (KBr) υ (cm^{-1}): 3444, 3327, 3212 (NH_2), 2195 (CN); ^1H NMR δ: 8.01–7.05 (m, 8H, aromatic), 7.15 (bs, 2H, NH_2), 5.75 (s, 1H, H-1); ^{13}C NMR δ: 159.70 (C-3), 147.82 (C-4a), 131.35 (C-10a), 130.88 (C-7), 130.15 (C-6a), 129.04 (C-6), 128.08 (C-8), 125.03 (C-10), 121.13 (C-10b), 119.47 (C-9), 117.49 (C-5), 113.72 (CN), 55.72 (C-2), 36.17 (C-1), 144.79, 132.10, 129.28, 129.22, 128.89 (aromatic); MS *m/z* (%): 450 ($M^+ + 6$, 6.27), 448 ($M^+ + 4$, 45.34), 446 ($M^+ + 2$, 100.00), 444 (M^+, 61.51) with a base peak at 446 (100); Anal. Calcd for $C_{20}H_{11}BrCl_2N_2O$: C, 53.84; H, 2.49; N, 6.28. Found: C, 53.91; H, 2.61; N, 6.40%.

*4.2.9. 3-Amino-9-bromo-1-(2,4-dichlorophenyl)-1H-benzo[f]chromene-2-carbonitrile (**4i**)*

Yellow crystals from ethanol; yield 87%; m.p. 290–291 °C; IR (KBr) υ (cm^{-1}): 3441, 3324, 3211 (NH_2), 2196 (CN); ^1H NMR δ: 8.01–7.06 (m, 8H, aromatic), 7.14 (bs, 2H, NH_2), 5.66 (s, 1H, H-1); ^{13}C NMR δ: 159.60 (C-3), 147.82 (C-4a), 131.59 (C-10a), 130.14 (C-7), 129.28 (C-6a), 128.91 (C-6), 128.09 (C-8), 125.00 (C-10), 121.13 (C-10b), 119.45 (C-9), 117.49 (C-5), 113.60 (CN), 55.78 (C-2), 34.77 (C-1), 141.36, 132.31, 131.89 131.31, 130.89, 128.58 (aromatic); MS *m/z* (%): 450 ($M^+ + 6$, 3.37), 448 ($M^+ + 4$, 25.22), 446 ($M^+ + 2$, 55.24), 444 (M^+, 33.89) with a base peak at 350 (100); Anal. Calcd for $C_{20}H_{11}BrCl_2N_2O$: C, 53.84; H, 2.49; N, 6.28. Found: C, 53.91; H, 2.54; N, 6.36%.

*4.2.10. 3-Amino-9-bromo-1-(2,5-dichlorophenyl)-1H-benzo[f]chromene-2-carbonitrile (**4j**)*

Colorless crystals from ethanol; yield 86%; m.p. 310–311 °C; IR (KBr) υ (cm^{-1}): 3440, 3323, 3210 (NH_2), 2197 (CN); ^1H NMR δ: 8.02–7.08 (m, 8H, aromatic), 7.18 (bs, 2H, NH_2), 5.67 (s, 1H, H-1); ^{13}C NMR δ: 159.65 (C-3), 147.84 (C-4a), 131.28 (C-10a), 130.27 (C-7), 129.96 (C-6a), 128.88 (C-6), 128.12 (C-8), 125.04 (C-10), 121.18 (C-10b), 119.39 (C-9), 117.53 (C-5), 113.18 (CN), 55.56 (C-2), 35.39 (C-1), 144.21, 132.57, 131.53, 130.91, 129.57, 129.28 (aromatic); ^{13}C NMR-DEPT spectrum at 135°CH, CH_3 [positive (up)], CH_2 [negative (down)], revealed the following signals at δ: 131.53 (aromatic ↑), 130.91 (aromatic ↑), 130.27 (C-7 ↑), 129.57 (aromatic ↑), 128.88 (C-6 ↑), 128.12 (C-8 ↑), 125.04 (C-10 ↑), 117.53 (C-5 ↑), 35.39 (C-1 ↑). In the DEPT spectrum at 90° only CH signals are positive (up) and showed δ: 131.53 (aromatic ↑), 130.91 (aromatic ↑), 130.27 (C-7 ↑), 129.57 (aromatic ↑), 128.88 (C-6 ↑), 128.12 (C-8 ↑), 125.04 (C-10 ↑), 117.53 (C-5 ↑), 35.39 (C-1 ↑). In the DEPT spectrum at 45° (CH, CH_2 and CH_3 positive) revealed signals at δ: 131.53 (aromatic ↑), 130.91 (aromatic ↑), 130.27 (C-7 ↑), 129.57 (aromatic ↑), 128.88 (C-6 ↑), 128.12 (C-8 ↑), 125.04 (C-10 ↑), 117.53 (C-5 ↑), 35.39 (C-1 ↑); ^{13}CNMR-APT spectrum CH, CH_3 [positive (up)], CH_2, Cq [negative (down)], revealed the following signals at δ: 159.65 (C-3 ↓), 147.84 (C-4a ↓), 144.21 (aromatic ↓), 132.57 (aromatic ↓),131.53 (aromatic ↑), 131.28 (C-10a ↓), 130.91(aromatic ↑), 130.27 (C-7 ↑), 129.96 (C-6a ↓), 129.57 (aromatic ↑), 129.28 (aromatic ↓), 128.88 (C-6 ↑), 128.12 (C-8 ↑), 125.04 (C-10 ↑), 121.18 (C-10b ↓), 119.39 (C-9 ↓), 117.53 (C-5 ↑), 113.18 (CN ↓), 55.56 (C-2 ↓), 35.39 (C-1 ↑); MS *m/z* (%): 450 ($M^+ + 6$, 7.88), 448 ($M^+ + 4$, 47.57), 446 ($M^+ + 2$, 100.00), 444 (M^+, 67.59) with a base peak at 446 (100); Anal. Calcd for $C_{20}H_{11}BrCl_2N_2O$: C, 53.84; H, 2.49; N, 6.28. Found: C, 53.78; H, 2.41; N, 6.19%.

*4.2.11. 3-Amino-9-bromo-1-(2,6-dichlorophenyl)-1H-benzo[f]chromene-2-carbonitrile (**4k**)*

Yellow crystals from ethanol/benzene; yield 85%; m.p. 319–320 °C; IR (KBr) υ (cm^{-1}): 3440, 3321, 3210 (NH_2), 2197 (CN); ^1H NMR δ: 8.00–7.28 (m, 8H, aromatic), 7.13 (bs, 2H, NH_2), 6.10 (s, 1H, H-1); ^{13}C NMR δ: 160.14 (C-3), 136.96 (C-4a), 131.51 (C-10a), 131.14 (C-7), 130.93 (C-6a), 129.91 (C-6), 127.75 (C-8), 124.96 (C-10), 120.95 (C-10b), 119.27 (C-9), 117.15 (C-5), 111.74 (CN), 52.71 (C-2), 35.08 (C-1), 148.62, 135.09, 134.35, 130.20, 129.12, 128.85 (aromatic); MS *m/z* (%): 450 ($M^+ + 6$, 4.93), 448 ($M^+ + 4$, 47.32), 446 ($M^+ + 2$, 100.00), 444 (M^+, 62.47) with a base peak at 446 (100); Anal. Calcd for $C_{20}H_{11}BrCl_2N_2O$: C, 53.84; H, 2.49; N, 6.28. Found: C, 53.90; H, 2.53; N, 6.35%.

*4.2.12. 3-Amino-9-bromo-1-(3,4-dichlorophenyl)-1H-benzo[f]chromene-2-carbonitrile (**4l**)*

Colorless crystals from ethanol; yield 84%; m.p. 245–246 °C; IR (KBr) υ (cm^{-1}): 3439, 3320, 3211 (NH_2), 2198 (CN); ^1H NMR δ: 8.06–7.12 (m, 8H, aromatic), 7.14 (bs, 2H, NH_2), 5.50 (s, 1H, H-1); ^{13}C NMR δ: 159.72 (C-3), 147.67 (C-4a), 131.22 (C-10a), 131.17 (C-7), 129.41 (C-6a), 128.78 (C-6), 127.27 (C-8), 125.64 (C-10), 121.16 (C-10b), 119.89 (C-9), 117.53 (C-5), 114.04 (CN), 56.92 (C-2), 36.48 (C-1), 146.43, 131.33, 130.74, 130.03, 129.44, 128.20 (aromatic); ^{13}C NMR-DEPT spectrum at 135°CH, CH_3 [positive (up)], CH_2 [negative (down)], revealed the following signals at δ: 131.17 (C-7 ↑), 130.74 (aromatic ↑), 130.03 (aromatic ↑), 128.78 (C-6 ↑), 128.20 (aromatic ↑), 127.27 (C-8 ↑), 125.64 (C-10 ↑), 117.53 (C-5 ↑), 36.48 (C-1 ↑). In the DEPT spectrum at 90° only CH signals are positive (up) and showed δ: 131.17 (C-7 ↑), 130.74 (aromatic ↑), 130.03 (aromatic ↑), 128.78 (C-6 ↑), 128.20 (aromatic ↑), 127.27 (C-8 ↑), 125.64 (C-10 ↑), 117.53 (C-5 ↑), 36.48 (C-1 ↑). In the DEPT spectrum at 45° (CH, CH_2 and CH_3 positive)

revealed signals at δ: 131.17 (C-7 ↑), 130.74 (aromatic ↑), 130.03 (aromatic ↑), 128.78 (C-6 ↑), 128.20 (aromatic ↑), 127.27 (C-8 ↑), 125.64 (C-10 ↑), 117.53 (C-5 ↑), 36.48 (C-1 ↑); ^{13}CNMR-APT spectrum CH, CH_3 [positive (up)], CH_2, Cq [negative (down)], revealed the following signals at δ: 159.72 (C-3 ↓), 147.67 (C-4a ↓), 146.43 (aromatic ↓), 131.33 (aromatic ↓), 131.22 (C-10a ↓), 131.17 (C-7 ↑), 130.74 (aromatic ↑), 130.03 (aromatic ↑), 129.44 (aromatic ↓), 129.41 (C-6a ↓), 128.78 (C-6 ↑), 128.20 (aromatic ↑), 127.27 (C-8 ↑), 125.64 (C-10 ↑), 121.16 (C-10b ↓), 119.89 (C-9 ↓), 117.53 (C-5 ↑), 114.04 (CN ↓), 56.92 (C-2 ↓), 36.48 (C-1 ↑), MS *m/z* (%): 450 (M^+ + 6, 0.43), 448 (M^+ + 4, 2.94), 446 (M^+ + 2, 6.43), 444 (M^+, 3.95) with a base peak at 303 (100); Anal. Calcd for $C_{20}H_{11}BrCl_2N_2O$: C, 53.84; H, 2.49; N, 6.28. Found: C, 53.78; H, 2.42; N, 6.20%.

4.2.13. 3-Amino-9-bromo-1-(3,5-dibromo-2-methoxyphenyl)-1H-benzo[f] chromene-2-carbonitrile (**4m**)

Colorless crystals from ethanol; yield 83%; m.p. 285–286 °C; IR (KBr) υ (cm^{-1}): 3442, 3319, 3210 (NH_2), 2202 (CN); ^{1}H NMR δ: 8.10–7.33 (m, 7H, aromatic), 7.20 (bs, 2H, NH_2), 5.52 (s, 1H, H-1), 3.77 (s, 3H, OCH_3); ^{13}C NMR δ: 160.15 (C-3), 147.40 (C-4a), 142.21 (C-10a), 131.44 (C-6a), 130.75 (C-7), 129.94 (C-6), 128.11 (C-8), 125.29 (C-10), 121.19 (C-10b), 118.24 (C-9), 117.58 (C-5), 114.29 (CN), 61.89 (CH_3), 56.04 (C-2), 33.59 (C-1), 153.26, 134.46, 131.74, 129.18, 120.33, 117.03 (aromatic); ^{13}C NMR-DEPT spectrum at 135°CH, CH_3 [positive (up)], CH_2 [negative (down)], revealed the following signals at δ: 134.46 (aromatic ↑), 131.74 (aromatic ↑), 130.75 (C-7 ↑), 129.94 (C-6 ↑), 128.11 (C-8 ↑), 125.29 (C-10 ↑), 117.58 (C-5 ↑), 61.89 (CH_3 ↑), 33.59 (C-1 ↑). In the DEPT spectrum at 90° only CH signals are positive (up) and showed δ: 134.46 (aromatic ↑), 131.74 (aromatic ↑), 130.75 (C-7 ↑), 129.94 (C-6 ↑), 128.11 (C-8 ↑), 125.29 (C-10 ↑), 117.58 (C-5 ↑), 33.59 (C-1). In the DEPT spectrum at 45° (CH, CH_2 and CH_3 positive) revealed signals at δ: 134.46 (aromatic ↑), 131.74 (aromatic ↑), 130.75 (C-7 ↑), 129.94 (C-6 ↑), 128.11 (C-8 ↑), 125.29 (C-10 ↑), 117.58 (C-5 ↑), 61.89 (CH_3 ↑), 33.59 (C-1 ↑); ^{13}CNMR-APT spectrum CH, CH_3 [positive (up)], CH_2, Cq [negative (down)], revealed the following signals at δ: 160.15 (C-3 ↓), 159.72 (C-3 ↓), 153.26 (aromatic ↓), 147.67 (C-4a ↓), 147.40 (C-4a ↓), 146.43 (aromatic ↓), 142.21 (C-10a ↓), 134.46 (aromatic ↑), 131.74 (aromatic ↑), 131.44 (C-6a ↓), 130.75 (C-7 ↑), 129.94 (C-6 ↑), 129.18 (aromatic ↓), 128.11 (C-8 ↑), 125.29 (C-10 ↑), 121.19 (C-10b ↓), 120.33 (aromatic ↓), 118.24 (C-9 ↓), 117.58 (C-5 ↑), 117.03 (aromatic ↓), 114.29 (CN ↓), 61.89 (CH_3 ↑), 56.04 (C-2 ↓), 33.59 (C-1 ↑); MS *m/z* (%): 450 (M^+ + 6, 5.33), 566 (M^+ + 4, 16.37), 564 (M^+ + 2, 16.61), 562 (M^+, 5.75) with a base peak at 532 (100); Anal. Calcd for $C_{21}H_{13}Br_3N_2O_2$: C, 44.64; H, 2.32; N, 4.96. Found: C, 44.73; H, 2.42; N, 5.07%.

4.3. Biological screening

4.3.1. Cell culture

The tumor cell lines breast adenocarcinoma (MCF-7), human colon carcinoma (HCT-116), and hepatocellular carcinoma (HepG-2) were obtained from the American Type Culture Collection (ATCC, Rockville, MD). The cells were grown on RPMI-1640 medium supplemented with 10% inactivated fetal calf serum and 50 μg/ml gentamycin. The cells were maintained at 37 °C in a humidified atmosphere with 5% CO_2 and were subculture two to three times a week.

4.3.2. Cytotoxicity evaluation using viability assay

The tumor cell lines were suspended in a medium at concentration 5 × 104 cells/well in Corning® 96-well tissue culture plates and then incubated for 24 h. The tested compounds with concentrations ranging from 0 to 50 μg/ml were then added into 96-well plates (six replicates) to achieve different concentration for each compound. Six vehicle controls with media or 0.5% DMSO were run for each 96 well plate as a control. After incubating for 24 h, the numbers of viable cells were determined by the MTT test. Briefly, the media was removed from the 96 well plates and replaced with 100 μl of fresh culture RPMI 1640 medium without phenol red then 10 μl of the 12 mM MTT stock solution (5 mg of MTT in 1 ml of PBS) to each well including the untreated controls. The 96-well plates were then incubated at 37 °C and 5% CO_2 for 4 h. An 85-μl aliquot of the media was removed from the wells, and 50 μl of DMSO was added to each well and mixed thoroughly with the pipette and incubated at 37 °C for 10 min. Then, the optical density was measured at 590 nm with the microplate reader (Sunrise, TECAN, Inc, USA) to determine the number of viable cells and the percentage of viability was calculated as [1 − (ODt/ODc)] × 100% where ODt is the mean optical density of wells treated with the tested sample and ODc is the mean optical density of untreated cells. The relation between surviving cells and drug concentration is plotted to get the survival curve of each tumor cell line after treatment with the specified compound. The 50% inhibitory concentration (IC_{50}), the concentration required to cause toxic effects in 50% of intact cells, was estimated from graphic plots of the dose response curve for each concentration [33-35].

4.3.3. Cell cycle assays

Cell cycle arrest and distribution were done using Propidium Iodide Flow Cytometry Kit (ab139418, Abcam) as previously described [43]. Human cancer cell lines (MCF-7, HCT-116, and HepG-2) at 1 × 10^4 cells were cultured in 60-mm dishes in the presence of various tested compounds with a concentration equal to the IC_{50} value for 24 h. Cells were collected and washed with PBS, fixed with precooled 70% ethanol at 4 °C. Staining went along in PBS containing 40 μg/ml RNase A and 10 μg/ml propidium iodide in the dark for 15 min. The DNA content in each cell nucleus was determined by a FACS Calibur flow cytometer (BD Biosciences, Franklin Lakes, NJ, USA). Finally, Cell cycle phase distribution was analyzed using Cell Quest Pro software (BD Biosciences) showing collected propidium iodide fluorescence intensity on FL2.

4.3.4. Annexin V-FITC apoptosis detection

Apoptosis assay was performed with an Annexin V-FITC/PI double staining apoptosis detection kit (K101, Biovison) using a flow cytometer [44]. Human Cells treated with different newly synthesized compounds (IC50 value) were harvested by trypsinization, washed twice with 4 °C PBS, and re-suspended in binding buffer. Annexin V-FITC and Propidium iodide (PI) solutions was then added to stain the cells before analysis by flow cytometry A minimum of 10,000 cells per sample were acquired. Annexin V-FITC binding (FL1) and PI (FL2) were analyzed using Cell Quest Pro software (BD Biosciences).

4.3.5. Topoisomerase I relaxation assay

Topoisomerase I catalytic activity was done using supercoiled (Form I) plasmid substrate according to the protocol provided by Topoisomerase I Assay Kit (TG1015-1A, TopoGEN, Inc., Florida, USA) [45,46]. Briefly, 1 unit of purified human topoisomerase I was added to the substrate with decreasing concentrations of c-MET reference drug and the different tested compounds (100, 50, 25, 12.5, and 6.3 μg/ml) for 30 min at 37 °C, the reaction was then stopped by addition stop buffer. The reaction mixture was analyzed on 1% agarose gel by electrophoresis prior to photo documentation.

4.3.6. KDNA decatenation activity of topoisomerase II

Topoisomerase II catalytic activity was done using kinetoplast DNA (kDNA) substrate according to the protocol provided by Topoisomerase II Assay Kit (TG1001-1A, TopoGEN, Inc., Florida, USA) [47,48]. Briefly, 200 ng of KDNA plus decreasing concentrations of c-MET reference drug and the different tested compounds (100, 50, 25, 12.5, and 6.3 μg/ml)was added to one unit of the human recombinant topoisomerase II at 37 °C for 30 min, then the reaction was stopped by addition stop buffer. The reaction mixture was analyzed on 1% agarose gel by electrophoresis prior to photo documentation.

4.3.7. Statistics

All data were expressed as the means ± standard deviation (SD), from at least three independent experiments with similar results. Statistical analysis and figures were performed by Graph Pad Prism 5.01 (Graph Pad Software, San Diego, CA. USA).

Acknowledgements

The authors extend their appreciation to the Deanship of Science Research at King Khalid University, Saudi Arabia for funding this work through General Research Project under Grant Number (R.G.P.1/111/40). In addition, the authors deeply thank the Regional Center for Mycology & Biotechnology (RCMP), Al-Azhar University, Cairo, Egypt, for carrying out the antitumor study, elemental analyses and also, for Mr. Ali Y. A. Alshahrani for drawing the ^{1}H NMR and ^{13}C NMR spectra.

Appendix A. Supplementary material

Supplementary data to this article can be found online at https://doi.org/10.1016/j.bioorg.2019.103289.

References

[1] L. Daviot, T. Len, C.S. Ki Lin, C. Len, Microwave-assisted homogeneous acid catalysis and chemoenzymatic synthesis of dialkyl succinate in a flow reactor, Catalysts 9 (2019) 272, https://doi.org/10.3390/catal9030272.
[2] S. Nain, R. Singh, S. Ravichandran, Importance of microwave heating in organic synthesis, Adv. J. Chem. A 2 (2019) 94–104.
[3] V.U. Mane, S.M. Chavan, B.R. Choudhari, D.V. Mane, Microwave assisted synthesis of tetrahydrobenzo[*b*]Pyrans Via one pot multicomponent reaction using [Et_3NH][HSO_4] as ionic liquid catalyst, J. Pharm. Chem. Biol. Sci. 6 (2019) 311–319.
[4] N. Sharma, U.K. Sharma, E.V. Van der Eycken, Microwave-assisted organic synthesis: overview of recent applications. Green techniques for organic synthesis and medicinal, Chemistry Ch17 (2018) 441–468, https://doi.org/10.1002/9781119288152.
[5] H. Takano, T. Narumi, W. Nomura, H. Tamamura, Microwave-assisted synthesis of azacoumarin fluorophores and the fluorescence characterization, J. Org. Chem. 82 (2017) 2739–2744.
[6] A. Chaker, E. Najahi, F. Nepveu, F. Chabchoub, Microwave-assisted synthesis of chromeno-[2,3-*d*]pyrimidinone derivatives, Arab. J. Chem.10 (2017) S3040–S3047.
[7] C.O. Kappe, D. Dallinger, Controlled microwave heating in modern organic synthesis: highlights from the 2004–2008 literature, Mol. Divers 13 (2009) 71–193.
[8] E.M. de Marigorta, J.M. de Los Santos, A.M.O. de Retana, J. Vicario, F. Palacios, Multicomponent reactions (MCRs): a useful access to the synthesis of benzo-fused γ-lactams, Beilstein J. Org. Chem. 15 (2019) 1065–1085.
[9] C.G. Neochoritis, T. Zhao, A. Dömling, Tetrazoles via multicomponent reactions, Chem. Rev. 119 (2019) 1970–2042.
[10] M. Leonardi, M. Villacampa, J.C. Menendez, Multicomponent mechanochemical synthesis, Chem. Sci. 9 (2018) 2042–2064.
[11] H.E.A. Ahmed, M.A.A. El-Nassag, A.H. Hassan, R.M. Okasha, S. Ihmaid, A.M. Fouda, T.H. Afifi, A. Aljuhani, A.M. El-Agrody, Introducing novel potent anticancer agents of 1H-benzo[f]chromene scaffolds, targeting c-Src kinase enzyme with MDA-MB-231 cell line anti-invasion effect, J. Enzyme Inhibit. Med. Chem. 33 (2018) 1074–1088.
[12] H.M. Mohamed, A.M. Fouda, E.S.A.E.H. Khattab, A.M. El-Agrody, T.H. Afifi, Synthesis, *in-vitro* cytotoxicity of 1*H*-benzo[*f*]chromene derivatives and structure–activity relationships of the 1-aryl group and 9-position, Z. Naturforsch. 72 (2017) 161–171.
[13] A.M. El-Agrody, A.-A.M. Al-Dies, A.M. Fouda, Microwave assisted synthesis of 2-amino-6-methoxy-4*H*-benzo[*h*]chromene derivatives, Eur. J. Chem. 5 (2014) 133–137.
[14] R. Pratap, V. Ji Ram, Natural and synthetic chromenes, fused chromenes, and versatility of dihydrobenzo[*h*]chromenes in organic synthesis, Chem. Rev. 114 (2014) 10476–10526.
[15] Synthesis and biological evaluation of some new 3-cyano-2-amino-substitutedchromene derivatives, Der Pharma Chemica 7 (2015) 117–129.
[16] J. Safari, M. Heydarian, Z. Zarnegar, Synthesis of 2-amino-7-hydroxy-4*H*-chromene derivatives under ultrasound irradiation: A rapid procedure without catalyst, Arab. J. Chem. 10 (2017) S2994–S3000.
[17] I. Gameiro, P. Michalska, G. Tenti, Á. Cores, I. Buendia, A.I. Rojo, N.D. Georgakopoulos, J.M. Hernández-Guijo, M.T. Ramos, G. Wells, M.G. López1, A. Cuadrado, J.C. Menéndez, R. León, Discovery of the first dual GSK3b inhibitor/Nrf2 inducer. A new multitarget therapeutic strategy for Alzheimer's disease, Sci. Rep. 7 (2017) 45701, https://doi.org/10.1038/srep45701.
[18] H.A. Oskooie, M.M. Heravi, N. Karimi, M.E. Zadeh, Caro's acid–silica gel: An efficient and versatile catalyst for the one-pot synthesis of tetrahydrobenzo[b]pyran derivatives synth, Commun. 41 (2011) 436–440.
[19] G. Pinna, G. Loriga, P. Lazzari, S. Ruiu, M. Falzoi, S. Frau, A. Pau, G. Muri-neddu, B. Asproni, G.A. Pinna, Eur. J. Med. Chem. 82 (2014) 281–292.
[20] A. Kheirollahi, M. Pordeli, M. Safavi, S. Mashkouri, M.R. Naimi-Jamal, S.K. Ardestani, Cytotoxic and apoptotic effects of synthetic benzochromene derivatives on human cancer cell lines, Naunyn-Schmiedeberg's Arch. Pharmacol. 387 (2014) 1199–1280.
[21] A.M. El-Agrody, A.M. Fouda, E.S.A.E.H. Khattab, Halogenated 2-amino-4*H*-benzo[*h*]-chromene derivatives as antitumor agents and the relationship between lipophilicity and antitumor activity, Med. Chem. Res. 26 (2017) 691–700.
[22] A.M. El-Agrody, A.H. Halawa, A.M. Fouda, A.M. Al-Dies, The antiproliferative activity of novel 4*H*-benzo[*h*]chromenes, 7H-benzo[*h*]chromeno[2,3-*d*]pyrimidines and the structure–activity relationships of the 2-,3-positions and fused rings at the 2,3-positions, J. Saudi Chem. Soc. 21 (2017) 82–90.
[23] M.E. Haiba, E.S. Al-Abdullah, H.A. Ghabbour, S.M. Riyadh, R.M. Abdel-Kader, Inhibitory activity of benzo[*h*]quinoline and benzo[*h*]chromene in human glioblastoma cells, Trop. J. Pharmaceut. Res. 15 (2016) 2337–2343.
[24] A. Rafinejad, A. Fallah-Tafti, R. Tiwari, A.N. Shirazi, D. Mandal, A. Shafiee, K. Parang, A. Foroumadi, T. Akbarzadeh, 4-Aryl-4*H*-naphthopyrans derivatives: one-pot synthesis, evaluation of Src kinase inhibitory and anti-proliferative activities, DARU J. Pharm. Sci. 20 (2012) 100–107.
[25] H.E.A. Ahmed, M.A.A. El-Nassag, A.H. Hassan, H.M. Mohamed, A.H. Halawa, R.M. Okasha, S. Ihmaid, S.M. Abd El-Gilil, E.S.A.E.H. Khattab, A.M. Fouda, A.M. El-Agrody, A. Aljuhani, T.H. Afifi, Developing lipophilic aromatic halogenated fused systems with specific ring orientations, leading to potent anticancer analogs and targeting the *c-Src* Kinase enzyme, J. Mol. Struct. 1186 (2019) 212–223.
[26] T.H. Afifi, R.M. Okasha, H.E.A. Ahmed, J. Ilas, T. Saleh, A.S. Abd-El-Aziz, Structure-activity relationships and molecular docking studies of chromene and chromene based azo chromophores: A novel series of potent antimicrobial and anticancer agents, EXCLI J. 16 (2017) 868–902.
[27] A.M. El-Agrody, H.K. Abd El-Mawgoud, A.M. Fouda, E.S.A.E.H. Khattab, Synthesis, in-vitro cytotoxicity of 4*H*-benzo[*h*]chromene derivatives and structure–activity relationships of 4-aryl group and 3-, 7-positions. Chem. Pap. 70 (2016) 1279–1292.
[28] L. Plazzi, A. Cavalli, F. Belluti, A. Bisi, S. Gobbi, S. Rizzo, M. Bartolini, V. Andrisano, M. Recanatini, A. Rampa, Extensive SAR and Computational Studies of 3-{4-[(Benzylmethyl-amino)methyl]phenyl}-6,7-dimethoxy-2*H*-2-chromenone (AP2238) Derivatives, J. Med. Chem. 50 (2007) 4250–4254.
[29] S. Gorle, S. Maddila, S.N. Maddila, K. Naicker, M. Singh, P. Singh, S.B. Jonnalagadda, Synthesis, molecular docking study and *in vitro* anticancer activity of tetrazole linked benzochromene derivatives, Anti-Cancer Agents Med. Chem. 17 (2017) 464–470.
[30] Y. Pommier, Topoisomerase I inhibitors: camptothecins and beyond, Nat. Rev. Cancer 6 (2006) 789–802.
[31] J.J. Champoux, DNA topoisomerases: structure, function, and mechanism, Annu. Rev. Biochem. 70 (2001) 369–413.
[32] S.M. Vos, E.M. Tretter, B.H. Schmidt, J.M. Berger, All tangled up: how cells direct, manage and exploit topoisomerase function, Nat. Rev. Mol. Cell Biol. 12 (2011) 827–841.
[33] T. Mosmann, Rapid colorimetric assay for cellular growth and survival: application to proliferation and cytotoxicity assays, J. Immunol. Methods 65 (1983) 55–63.
[34] A.U. Rahman, M.I. Choudhary, W.J. Thomsen, Bioassay Technique for Drug Development, Harwood Academic Publishers, Reading, UK, 2001.
[35] F. Demirci, K.H.C. Başer, Bioassay Techniques for Drug Development By A.U. Rahman, M.I. Choudhary (HEJRIC, University of Karachi, Pakistan), William J. Thomsen (Areana Pharmaceuticals, San Diego, CA). Harwood Academic Publishers, Amsterdam, The Netherlands. 2001. xii + 223 pp. 15.5 × 23.5 cm. $79.00. ISBN 90-5823-051-1, J. Natural Prod. 65 (2002) 1086–1087.
[36] G.K. Schwartz, M.A. Shah, Targeting the cell cycle: a new approach to cancer therapy, J. Clin. Oncol. 23 (2005) 9408–9421.
[37] G.H. Williams, K. Stoeber, The cell cycle and cancer, J. Pathol. 226 (2012) 352–364.
[38] V.A. Fadok, D.R. Voelker, P.A. Campbell, J.J. Cohen, D.L. Bratton, P.M. Henson, Exposure of phosphatidylserine on the surface of apoptotic lymphocytes triggers specific recognition and removal by macrophages, J. Immunol. 1 (1992) 2207–2216.
[39] J.H. Liu, Activation of apoptosis pathways by different classes of anticancer drugs, Hubei: University of Ulm, http://vts.uni-ulm.de/docs/2001/798/vts_798.pdf, 2001.
[40] Y.S. Tor, L.S. Yazan, J.B. Foo, N. Armania, Y.K. Cheah, R. Abdullah, M.U. Imam, N. Ismail, Ismail M, Induction of apoptosis through oxidative stress-related pathways in MCF-7, human breast cancer cells, by ethyl acetate extract of Dilleniasuffruticosa, BMC Complement Altern. Med. 14 (2014) 55.
[41] X. Cai, P.J. Gray Jr, D.D. Von Hoff, DNA minor groove binders: back in the groove, Cancer Treat Rev. 35 (2009) 437–450.
[42] P.M. O'Connor, K.W. Kohn, A fundamental role for cell cycle regulation in the chemosensitivity of cancer cells? Sem. Cancer Biol. 3 (1992) 409–416.
[43] L.L. Vindelov, I.L. Christensen, N.I. Nissen, Standardization of high-resolution flow cytometric DNA analysis by the simultaneous use of chicken and trout red blood cells as internal reference standards, Cytometry 3 (1983) 328–331.
[44] G. Zhang, V. Gurtu, S.R. Kain, G. Yan, Early detection of apoptosis using a fluorescent conjugate of Annexin V, Biotechniques 23 (1997) 525–531.
[45] T.S. Dexheimer, Y. Pommier, DNA cleavage assay for the identification of topoisomerase I inhibitors, Nature 3 (2008) 1736–1750.
[46] L. Zhang, P. Sullivan, J. Suyama, Epidermal growth factor-induced heparanase nucleolar localization augments DNA topoisomerase I activity in brain metastatic breast cancer, Mol. Cancer Res. 8 (2010) 278–290.
[47] J.J. Bower, G.F. Karaca, Y. Zhou, D.A. Simpson, M. Cordeiro-Stone, W.K. Kaufman, Topoisomerase IIa maintains genomic stability through decatenation G2 checkpoint signaling, Oncogene 29 (2010) 4787–4799.
[48] M. Polycarpou-Schwarz, K. Müller, S. Denger, A. Riddell, J. Lewis, F. Gannon, G. Reid, R.G. Thanatop, A Novel 5-Nitrofuran that is a highly active, cell-permeable inhibitor of topoisomerase II, Cancer Res. 67 (2007) 4451–4458.